Miniature Plasmonic Wave Plates

Aurélien Drezet, Cyriaque Genet, and Thomas W. Ebbesen

ISIS, Louis Pasteur University, 8 allée Gaspard Monge, 67000, Strasbourg, France

(Received 11 January 2008; revised manuscript received 17 June 2008; published 24 July 2008)

Linear birefringence, as implemented in wave plates, is a natural way to control the state of polarization of light. We report on a general method for designing miniature planar wave plates using surface plasmons. The resonant optical device considered here is a single circular aperture surrounded by an elliptical antenna grating. The difference between the short and long axis of each ellipsis introduces a phase shift on the surface plasmons which enables the realization of a quarter wave plate. Furthermore, the experimental results and the theoretical analysis show that the general procedure used does not influence the optical coherence of the polarization state and allows us to explore completely the surface of the unit Poincaré sphere by changing only the shape of the elliptical grating.

DOI: 10.1103/PhysRevLett.101.043902 PACS numbers: 42.25.Lc, 42.70.−a, 73.20.Mf

Surface plasmon polaritons (SPPs), electromagnetic surface waves existing at the interface between a dielectric and a metal [1], are particularly sensitive to tiny variations in their local electronic environments. This creates new opportunities and applications for photonics [2] by simply texturing a metal surface. For example, metal films structured with two-dimensional subwavelength hole arrays present remarkable properties such as the extraordinary optical transmission (EOT), which is a clear signature of SPP-light interaction [3–5]. In this particular context, several studies have started to address polarization issues, discussing in this respect the influence of the individual hole shapes. Elliptical or rectangular apertures can behave like polarizers, following the Malus law of absorption [6–8] (see also Ref. [9] for similar work on elliptical nanoparticles). However, these structures do not display linear birefringence. Linear birefringence is absolutely central in optics since it allows full control of the state of polarization (SOP) of light without absorption. A half wave plate rotates the plane of polarization while a quarter wave plate converts linear polarized light into a circular one, the combination of the two enabling a complete exploration of all polarization states.

In this Letter, we report for the first time, both experimentally and theoretically, the design and characterization of a plasmonic optical wave plate. In order to obtain the linear birefringence, we have developed a modified version of the single circular nanoaperture surrounded by periodic circular corrugations, also known as a *bull's eye* structure [10]. Such an optical grating acts as a miniature antenna presenting huge EOT for the optical wavelength inside a narrow band centered on the SPP resonance [10,11]. The specificity of the structure presented here is its unique ability to control the SOP of the electromagnetic field going through the aperture. This is achieved by introducing a well-defined eccentricity in the grating geometry which in turn modifies the phase of the excited SPP and consequently the polarization of the transmitted light. This resembles in a wide sense the phase matching in distributed feedback lasers (DFB). To fully characterize the optical behavior of our device, a genuine polarization tomography of the isolated subwavelength aperture had to be implemented. Furthermore, we have developed a microscopic (dipolar) model to link structural design with change of SOP.

Besides its fundamental interest, such control over the SOP can be used broadly in photonic applications requiring local addressing, e.g., detectors [12], displays [11], and compact circular polarization antennas [13]. In addition, ultrafast optomagnetic data storage has been demonstrated with femtosecond lasers and circularly polarized light [14]. The device demonstrated here creates both the right helicity and the large fields in a tiny volume favorable for such purposes.

For our experiments we consider a bull's eye structure made of 8 grooves and fabricated by focus-ion-beam milling in a 300 nm thick Au film (Fig. 1). The hole diameter is 260 nm and the groove's width and depth are 370 and 80 nm, respectively. The groove shape is chosen to be elliptical with the long axis $a_n = nP + P/4$ and the short axis $b_n = nP$. Here $P = 760$ nm is the period of the grating (which equals the SPP wavelength λ_{SPP} for a laser excitation at 785 nm [15]) and n is an integer going from 1 to 8 [see Fig. 1(a)]. Also shown in Fig. 1(b) is the transmission spectra of the structure with a resonant peak at $\lambda_0 \simeq 777$ nm. The measured extraordinary transmission efficiency (larger than 1) is a direct signature of the involvement of SPP [2]. The presence of this transmission peak proves that, despite the small increment of $\delta L = P/4$ between the long and short axis of the ellipses, the structure still behaves like a miniature antenna. We can justify our choice for the grating symmetry on theoretical grounds. In our model we discretize the grooves into a sum of point dipoles $\mathbf{P}_M$ proportional to the local electric field at M. Each dipole is excited coherently by the light impinging normal to the metal film and SPPs are launched in the direction of the central nanohole where they excite an in-plane radiating dipole [16]. To reproduce completely the

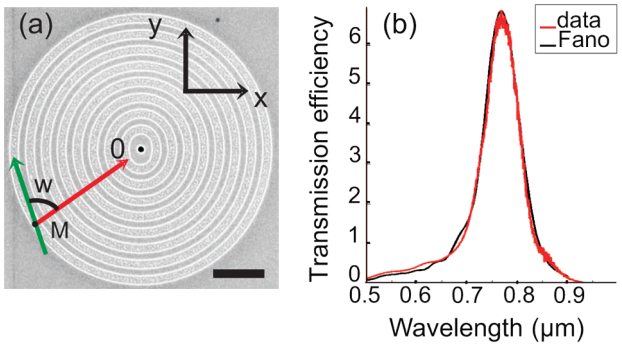

FIG. 1 (color). (a) Scanning electron microscopy image of the elliptical bull's eye structure. The scale bar is 2 μm long. The green arrow is an excited point dipole $\mathbf{P}_M$ located in **M**. SPP (red arrow) launched in **M** propagates along the radial direction **MO** to reach the hole located in **O**. w is the angle between **MO** and $\mathbf{P}_M$. (b) Comparison between the experimental white light transmission spectrum (red curve) associated with the structure shown in (a) and the theoretical prediction (black curve) obtained with the 2D dipoles model. The transmission scale is dimensionless and corresponds to the ratio between the transmitted and the incoming power at the level of the aperture.

system, we introduce a second transmission channel in which the central dipole is excited directly by the incident light. The interference between these two channels leads to a Fano-like effect [17] resulting in the observed transmission peak. The relative (complex) amplitude between these two channels was fitted to reproduce the spectra of Fig. 1(b) [18]. The good agreement between our model and the data [see Fig. 1(b)] allows us to use it for predicting the optical behavior of the structure at a given λ. The principle of the device can be illustrated by considering only the point dipoles located along the short and long axes of the ellipses. It is thus clear that δL corresponds to a phase shift $\phi_{\mathrm{SPP}} = 2\pi\delta L/\lambda_{\mathrm{SPP}} = \pi/2$ between SPPs propagating along the long (y) and the short (x) axes. Additionally, the coupling between the incident light and SPPs depends on the cosine of the angle w between the radial vector **MO** and $\mathbf{P}_M$ [Fig. 1(a)]. It means that if the incident linear polarization is switched from a direction parallel to the x axis to a direction parallel to the y axis, the radiating central dipole will change from $\alpha\hat{\mathbf{x}}$ (where α is a constant) to $e^{i\pi/2}\alpha\hat{\mathbf{y}}$. From the point of view of this idealized picture (which neglects damping), we deduce that the system behaves like a birefringent biaxial medium, i.e., a perfect quarter wave plate, with fast and slow axes parallel, respectively, to the x and y axes. Obviously if we now take into account all the dipoles as well as the Fano interference effect and the finite value of the SPP propagation length L_{SPP} (damping) in the structure, the actual result will naturally deviate from this idealized case [19,20].

In order to study experimentally the SOP conversion by our structure, we carried out a complete polarization tomography [21] using the optical setup sketched in Fig. 2(a). A laser beam at $\lambda = 785$ nm is focused normally onto the structure by using an objective L_1. The transmitted light is collected by a second objective L_2 forming an Airy spot on the camera [see Figs. 2(b) and 2(c)] as expected since the hole behaves like a point source in an opaque gold film. In our experiments, the intensity is thus defined by taking the maximum of the Airy spot shown on Fig. 2(b). The SOP of light is prepared and analyzed with half wave plates, quarter wave plates, and polarizers located before and after the objectives [21–23]. We recall that the complete knowledge of the SOP require 6 intensity projection measurements $\langle I_{\hat{\mathbf{a}}_i}\rangle = \langle|\mathbf{E}\cdot\hat{\mathbf{a}}_i|^2\rangle$ made along the 4 linear polarization vectors $\hat{\mathbf{x}}$, $\hat{\mathbf{y}}$, $\hat{\mathbf{p}} = (\hat{\mathbf{x}} + \hat{\mathbf{y}})/\sqrt{2}$, $\hat{\mathbf{m}} = (\hat{\mathbf{x}} - \hat{\mathbf{y}})/\sqrt{2}$, and along the two circular polarization vectors $\hat{\mathbf{L}} = (\hat{\mathbf{x}} + i\hat{\mathbf{y}})/\sqrt{2}$, $\hat{\mathbf{R}} = (\hat{\mathbf{x}} - i\hat{\mathbf{y}})/\sqrt{2}$. It is convenient [22] to introduce the four Stokes parameters $S_1 = \langle I_{\hat{\mathbf{x}}} - I_{\hat{\mathbf{y}}}\rangle$ $S_2 = \langle I_{\hat{\mathbf{p}}} - I_{\hat{\mathbf{m}}}\rangle$, $S_3 = \langle I_{\hat{\mathbf{L}}} - I_{\hat{\mathbf{R}}}\rangle$, and $S_0 = \langle I_{\hat{\mathbf{x}}} + I_{\hat{\mathbf{y}}}\rangle = \langle I_{\mathrm{total}}\rangle$. The goal of this polarization tomography is then the determination of the 4×4 Mueller matrix $\mathcal{M}$ characterizing the transformation of the input Stokes parameters during the interaction of the laser light with the structure. In order to write down the full Mueller matrix, we measured 6×6 intensity projections corresponding to the 6 previously mentioned unit vectors for the input and the output polarizations [24].

At first, the isotropy of the bare setup was checked by measuring the Mueller matrix $\mathcal{M}^{\mathrm{glass}}$ with a glass substrate. Up to a normalization constant, we deduced that $\mathcal{M}^{\mathrm{glass}}$ is practically identical to the identity matrix $\mathcal{I}$ with

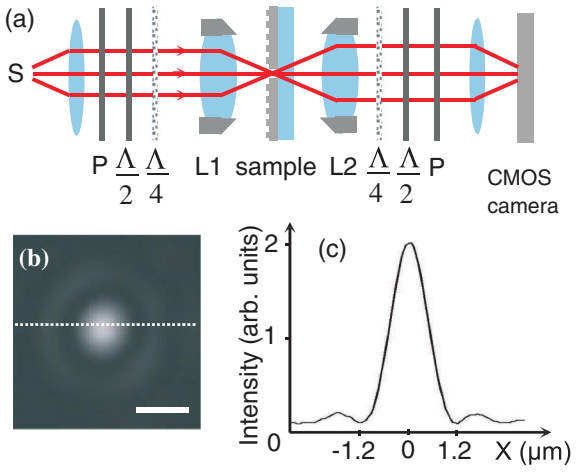

FIG. 2 (color). (a) Sketch of the optical polarization tomography setup. P, $\Lambda/4$, $\Lambda/2$ are, respectively, polarizers, quarter wave plates, and half wave plates located in the input and output beams. The image is recorded with a complementary metal oxide semiconductor (CMOS) camera and the light source S is a laser diode emitting at $\lambda = 785$ nm. L_1 and L_2 are two objective lenses ($\times 50$, NA $= 0.55$) and ($\times 40$, NA $= 0.6$), respectively. (b) Typical camera image of the light transmitted through our structure (the scale bar is 2 μm). (c) Cross cut of the intensity profile along the white dotted line shown in (b).

individual elements deviating from it by no more than 0.02. It implies that the optical setup does not induce depolarization and that consequently we can rely on our measurement procedure for obtaining $\mathcal{M}$. Optical depolarization (i.e., losses in polarization coherence) can be precisely quantified through the degree of purity of the Mueller matrix defined by [25] $D(\mathcal{M}) = (\frac{\mathrm{Tr}[\mathcal{M}^\dagger \mathcal{M}] - \mathcal{M}_{00}^2}{3\mathcal{M}_{00}^2})^{1/2} \leq 1$. We find $D(\mathcal{M}^{\mathrm{glass}}) = 0.9851$. We impute the residual depolarization ($1 - D \sim 2\%$) to the lenses and to alignment errors. It should be noted that the incident illumination spot size on the sample was varied between 2 and 20 μm without affecting the matrix, i.e., without introducing additional depolarization. In the following experiment, we consider the case of a large Gaussian spot with FWHM = 20 μm in order to illuminate the whole structure [26]. We then measured the Mueller matrix of our structure and found that

$$\mathcal{M}^{\mathrm{expt}} = \begin{pmatrix} \underline{1}.000 & \underline{0}.107 & -0.008 & 0.000 \\ \underline{0}.111 & \underline{0}.972 & -0.002 & -0.004 \\ 0.004 & -0.002 & \underline{0}.306 & \underline{-0.932} \\ 0.001 & -0.017 & \underline{0}.934 & \underline{0}.294 \end{pmatrix}, \quad (1)$$

which is clearly block diagonal, up to experimental errors. It is also remarkable that we have $D(\mathcal{M}^{\mathrm{expt}}) = 0.981$. This means that despite the existence of the SPP transmission channel, the polarization coherence is not lost during the propagation through the structure. This situation contrasts with previous SOP tomography measurements on metallic hole arrays in which the polarization degrees of freedom were mixed with spatial information responsible for SPP-induced depolarization [27]. Beside these two points, the matrix $\mathcal{M}^{\mathrm{expt}}$ exhibits several interesting symmetrical features which relate to the polarization properties of the device. First, it can be observed that in our experimental procedure the polarization in the Airy spot [see Fig. 2(b)] is homogeneous [28]. This means that in our analysis we are actually doing the polarization tomography of the central radiating dipole; i.e., we are dealing only with the SU(2) point symmetry of the Mueller matrix. In such a context, the rectangular point symmetry group C_{2v} of the ellipse imposes that the (2×2) Jones matrix [22] $\mathcal{J}$ connecting the incident electric field (E_x^{in}, E_y^{in}) to the transmitted electric field (E_x^{out}, E_y^{out}) must be diagonal in the x and y basis, i.e.,

$$\mathcal{J} \propto \begin{pmatrix} 1 & 0 \\ 0 & \beta \end{pmatrix},$$

where $\beta = \rho e^{i\phi}$ is a complex number. In analogy with bulk optics, ρ and ϕ measure, respectively, the relative dichroism (i.e., the relative absorption) and the birefringence of this biaxial 2D medium. Clearly ϕ is reminiscent of ϕ_{SPP} discussed above. Using $\mathcal{J}$ we obtain the theoretical Mueller matrix

$$\mathcal{M}^{C_{2v}} \propto \begin{pmatrix} 1+\rho^2 & 1-\rho^2 & 0 & 0 \\ 1-\rho^2 & 1+\rho^2 & 0 & 0 \\ 0 & 0 & 2\,\mathrm{Re}(\beta) & -2\,\mathrm{Im}(\beta) \\ 0 & 0 & 2\,\mathrm{Im}(\beta) & 2\,\mathrm{Re}(\beta) \end{pmatrix}, \quad (2)$$

which is similar to $\mathcal{M}^{\mathrm{expt}}$ and, in particular, satisfies the symmetries $\mathcal{M}_{01} = \mathcal{M}_{10}$, $\mathcal{M}_{00} = \mathcal{M}_{11}$, $\mathcal{M}_{22} = \mathcal{M}_{33}$, and $\mathcal{M}_{23} = -\mathcal{M}_{32}$ observed experimentally. We deduce $\rho = (\frac{\mathcal{M}_{00} - \mathcal{M}_{01}}{\mathcal{M}_{00} + \mathcal{M}_{01}})^{1/2}$ and $\tan\phi = \mathcal{M}_{32}/\mathcal{M}_{22}$. Using Eqs. (1) and (2) we obtain $\rho \simeq 0.898$ and $\phi \simeq 72.5°$. Reciprocally by injecting the previous values for ρ and ϕ in $\mathcal{M}^{C_{2v}}$ the result does not differ from $\mathcal{M}^{\mathrm{expt}}$ by more than 2%, in agreement with the value obtain for the residual depolarization. Then, using the fitting parameters already considered in the transmission spectrum Fig. 1(b), we numerically calculate the Mueller matrix predicted by the 2D dipole model and obtain

$$\mathcal{M}^{\mathrm{2D}} = \begin{pmatrix} 1.000 & 0.089 & 0.000 & 0.000 \\ 0.089 & 1.000 & 0.000 & 0.000 \\ 0.000 & 0.000 & 0.446 & -0.890 \\ 0.0000 & 0.000 & 0.890 & 0.446 \end{pmatrix}, \quad (3)$$

which is close to $\mathcal{M}^{C_{2v}}$ and $\mathcal{M}^{\mathrm{expt}}$ and corresponds to $D(\mathcal{M}^{\mathrm{2D}}) = 1$. This numerical model is sensitive to small variations of the fitting parameters and the agreement with the experiment could be probably improved by going beyond the paraxial approximation for the incident light [26].

Finally, we considered more closely the consequence of the transformation defined by $\mathcal{M}^{\mathrm{expt}}$ by varying the linear polarization θ of the input state every 10° from −90° to +90°. In Fig. 3(a) we show the transmitted intensity analyzed along the 6 fundamental polarizations $\hat{\mathbf{x}}$, $\hat{\mathbf{y}}$, $\hat{\mathbf{p}}$, $\hat{\mathbf{m}}$, $\hat{\mathbf{L}}$, and $\hat{\mathbf{R}}$ as a function of θ. The interference fringes observed are compared with the predictions given by the 2D dipole model (dotted curves) and with the intensity deduced from the Mueller matrix $\mathcal{M}^{\mathrm{expt}}$ (continuous curves). In both cases the agreement is very good, showing once again the consistency of the different measurements and deductions. Furthermore, this can be geometrically illustrated by using the Stokes vector [22] defined by $\mathbf{S} = [S_1\hat{\mathbf{x}} + S_2\hat{\mathbf{y}} + S_3\hat{\mathbf{z}}]/S_0$. The surface drawn by the input Stokes vector is called a Poincaré sphere and has the radius $D = 1$. As shown in Fig. 3(b) the operator $\mathcal{M}^{\mathrm{expt}}$ defines a geometrical transformation connecting this Poincaré sphere to an output surface with a characteristic radius $D(\mathcal{M}^{\mathrm{expt}})$. This experimental surface is very close to the ideal sphere $D = 1$ in agreement with the absence of net depolarization as discussed earlier. The experiment shown in Fig. 3(a) is also represented on this sphere. From Eq. (2), we deduce that if the input Stokes vector explores the equator corresponding to linear polarizations, the output Stokes vector draws a circle of radius $D \simeq 1$ which is contained in the plane $y/z = \mathcal{M}_{33}/\mathcal{M}_{32}$ making the angle

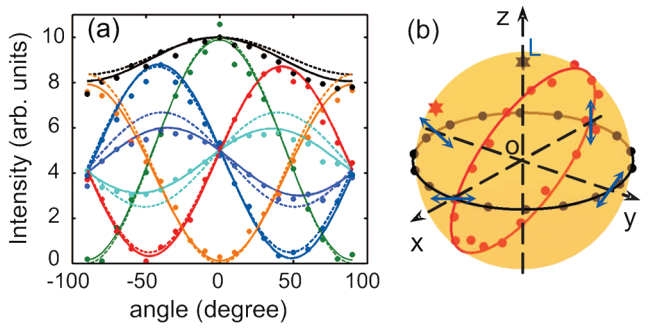

FIG. 3 (color). (a) SOP analysis of the output beam for a linearly polarized input beam. The polarization angle is measured relative to the x axis. Data points are compared to Eq. (1) (continuous curves) and to predictions of Eq. (3) (dotted curves). The colors black, green, orange, cyan, magenta, red, and blue correspond, respectively, to I_{total}, $I_{\hat{\mathbf{x}}}$, $I_{\hat{\mathbf{y}}}$, $I_{\hat{\mathbf{p}}}$, $I_{\hat{\mathbf{m}}}$, $I_{\hat{\mathbf{L}}}$, and $I_{\hat{\mathbf{R}}}$. (b) Image of the input Poincaré sphere through the transformation $\mathcal{M}^{\text{expt}}$ (yellow sphere). The black and red data points are, respectively, the input and output Stokes vectors associated with the experiment shown in (a). The circle represents the predictions deduced from $\mathcal{M}^{\text{expt}}$. The device also converts an input L state (black) star into a state shown by a red star.

$90° - \phi = 17.5°$ with the z axis. These predictions are directly consistent with the observations. Additionally, for a pure left circular input SOP, we experimentally obtain $\mathbf{S}^{\text{expt}} = 0.1123\hat{\mathbf{x}} - 0.8984\hat{\mathbf{y}} + 0.3104\hat{\mathbf{z}}$ in agreement with the value deduced from $\mathcal{M}^{C_{2v}}$: $\mathbf{S}^{C_{2v}} = 0.1067\hat{\mathbf{x}} - 0.9272\hat{\mathbf{y}} + 0.2949\hat{\mathbf{z}}$.

To conclude, all this experimental and theoretical analysis demonstrates that we have a clear understanding of the SPP structure considered here. First, we have $\rho \simeq 1$ which implies that the system acts essentially as a birefringent medium with the Jones matrix

$$\mathcal{J} \simeq \begin{pmatrix} 1 & 0 \\ 0 & e^{i\phi} \end{pmatrix},$$

i.e., a wave plate. Second, the value obtained for ϕ shows that the system differs slightly from an ideal quarter wave plate for which $\phi = 90°$. From the point of view of the Poincaré sphere, this angle measures directly the inclination of the output circle shown in Fig. 3(b). For a perfect quarter wave plate this circle will go through the poles; i.e., a complete conversion from linear to circular polarization will become possible if the input SOP is polarized along $\hat{\mathbf{p}}$ or $\hat{\mathbf{m}}$. In this context, numerical calculations with the 2D dipoles model show that by changing slightly the value for the long axis increment δL we can change the phase ϕ continuously. This means that with such a SPP device we can in principle tailor and generate any kind of SOP conversion on the Poincaré sphere going from the equator (linear polarization) to the poles (circular polarization) or vice versa. We expect that the SPP control over the polarization presented in this Letter could have many applications in photonics and in information storage technology.

The authors acknowledge financial support from the EC under project No. IST-FP6-034506.

[1] H. Raether, *Surface Plasmons* (Springer, Berlin, 1988).
[2] C. Genet and T. W. Ebbesen, Nature (London) **445**, 39 (2007).
[3] T. W. Ebbesen *et al.*, Nature (London) **391**, 667 (1998).
[4] W. L. Barnes *et al.*, Phys. Rev. Lett. **92**, 107401 (2004).
[5] L. Martín-Moreno *et al.*, Phys. Rev. Lett. **86**, 1114 (2001).
[6] R. Gordon *et al.*, Phys. Rev. Lett. **92**, 037401 (2004).
[7] J. Elliott *et al.*, Phys. Rev. B **70**, 233403 (2004).
[8] A. Degiron *et al.*, Opt. Commun. **239**, 61 (2004).
[9] W. Gotschy *et al.*, Opt. Lett. **21**, 1099 (1996).
[10] H. J. Lezec *et al.*, Science **297**, 820 (2002).
[11] E. Laux *et al.*, Nat. Photon. **2**, 161 (2008).
[12] T. Ishi *et al.*, Jpn. J. Appl. Phys. **44**, L364 (2005).
[13] G. Smith, *An Introduction to Classical Electromagnetic Radiation* (Cambridge University Press, Cambridge, England, 1997).
[14] C. D. Stanciu *et al.*, Phys. Rev. Lett. **99**, 047601 (2007).
[15] P. B. Johnson and R. W. Christy, Phys. Rev. B **6**, 4370 (1972).
[16] C. Genet, M. P. van Exter, and J. P. Woerdman, J. Opt. Soc. Am. A **22**, 998 (2005).
[17] C. Genet, M. P. van Exter, and J. P. Woerdman, Opt. Commun. **225**, 331 (2003).
[18] Additionally we modeled the transmission spectra of the central isolated hole alone by using a fit of experimental spectrum.
[19] D. S. Kim *et al.*, Phys. Rev. Lett. **91**, 143901 (2003).
[20] In our model we used $L_{\text{SPP}} = 0.95\ \mu$m to fit Fig. 2(b). This value agrees with the formula [19] $L_{\text{SPP}} = \lambda_0^2/(2\pi n_{\text{SPP}} \times \text{FWHM}) \simeq 0.93\ \mu$m where $n_{\text{SPP}} \simeq 1.05$ is the SPP index and FWHM is the full width at half maximum of the transmission peak.
[21] F. Le Roy-Brehonnet and B. Le Jeune, Prog. Quantum Electron. **21**, 109 (1997).
[22] M. Born and E. Wolf, *Principles of Optics* (Cambridge University Press, Cambridge, England, 1999), 7th ed.
[23] Y. Gorodetski *et al.*, Opt. Lett. **30**, 2245 (2005).
[24] Actually only 16 measurements are needed to determine $\mathcal{M}$ [21]. Our systematic procedure is thus more than sufficient to obtain $\mathcal{M}$.
[25] J. J. Gill, J. Opt. Soc. Am. A **17**, 328 (2000).
[26] For spot size FWHM $\simeq 20\ \mu$m the effective numerical aperture of the incident beam at $\lambda = 785$ nm is only $\lambda/\text{FWHM} \simeq 0.04$. At this low numerical aperture regime, the parameters used for the fit of the 2D dipole model at normal incidence are still pertinent.
[27] E. Altewischer *et al.*, Opt. Lett. **30**, 90 (2005).
[28] Given the fact that $\mathcal{M}^{\text{glass}} \simeq \mathcal{I}$, this is directly verified by using a pair of crossed polarizers in the input and output beam, i.e., measuring the extinction.